Eur. Phys. J. Special Topics **146**, 71–86 (2007)

DOI: 10.1140/epjst/e2007-00170-3

THE EUROPEAN PHYSICAL JOURNAL SPECIAL TOPICS

Domain wall dynamics: Growth laws, localized structures and stable droplets

D. Gomila[1,a], P. Colet[1,b], M.S. Miguel[1,c], and G.-L. Oppo[2,d]

[1] Instituto Mediterráneo de Estudios Avanzados (IMEDEA, CSIC-UIB), Campus Universitat Illes Balears, 07122 Palma de Mallorca, Spain
[2] SUPA, Department of Physics, University of Strathclyde, 107 Rottenrow, Glasgow G4 0NG, Scotland

Abstract. We discuss the relation between the dynamics of walls separating two equivalent domains and the existence of different kinds of localized structures in systems far from thermodynamic equilibrium. In particular we focus in systems displaying a modulational instability of a flat front where an amplitude equation for the dynamics of the curvature allows to characterize different growth regimes and to predict the existence of stable droplets, localized structures whose stability comes from nonlinear curvature effects.

1 Introduction

Localized structures (LS), or dissipative solitons, are commonplace in extended systems displaying bistability between either a periodic pattern and a homogeneous state or two homogeneous solutions. In 1D, the existence of such LS can be explained through a pinning mechanism around the "Maxwell" point where a front between the two stable solutions is at rest [1,2]. In the case of bistability between two equivalent homogeneous solutions, for instance as a result of a pitchfork bifurcation, the "Maxwell" point spread over all the bistable parameter region and the front is always at rest due to symmetry. In this case, the existence of LS in 1D due to the locking of two fronts through the interaction of their oscillatory tails is greatly enhanced. In 2D, however, the role of the curvature of the fronts has not been completely understood in these terms. Reversibility, which is the basic ingredient behind the pinning around a "Maxwell" point, is broken when studying a radial equation describing a circular domain wall. Moreover, the "Maxwell" point itself is destroyed by the curvature driven motion, even in the case of bistability between equivalent solutions. The extension of the 1D theory to 2D is, then, not straightforward.

On the other hand, the dynamics of such LS is strongly related the growth of spatial domains of one homogeneous solution embedded in the other. The study of domain wall dynamics provides, then, a different approach to study the formation of LS. For systems approaching thermodynamic equilibrium, domain growth has been studied long ago [3,4]. The physical mechanisms explaining the different asymptotic growth laws have been clearly identified. It is convenient to consider domain growth in systems with conserved and nonconserved order parameters separately. In the first case, one talks of spinodal decomposition leading to the Lifshitz–Slyozov $t^{1/3}$ power law. In the second case, the dominant mechanism is curvature driven minimization of surface tension energy, leading to the Allen–Cahn (AC) $t^{1/2}$ power

[a] e-mail: damia@imedea.uib.es
[b] e-mail: pere@imedea.uib.es
[c] e-mail: maxi@imedea.uib.es
[d] e-mail: gianluca@phys.strath.ac.uk

law [5]. In systems that do not approach thermodynamic equilibrium there is only a partial understanding of a variety of possible situations [6–9]. Reported results have been in some cases even contradictory. For example, in nonlinear optical systems several growth laws, including $t^{1/2}$ [10,11] and $t^{1/3}$ [12,13] have been reported. These results were obtained from numerical simulations but only in [10,11] evidence of scaling was given.

We have recently developed a quite general theory [14] to analyze the transition from a coarsening regime characterized by a $t^{1/2}$ growth law to one of labyrinthine pattern formation due to a modulational instability of a flat domain wall connecting two equivalent homogeneous solutions. Such transition has been observed experimentally in reaction diffusion [15,16] and optical [17] systems, and numerically in [10], as well as in Swift–Hohenberg models [18,19]. On the basis of our general theory, it is possible to show for which parameter regions there is dynamical scaling, so that, the growth follows a power law, and for which parameters there is no dynamical scaling. Furthermore the theory predicts a novel kind of localized structures, the stable droplets, large circular domain of one phase embedded in the other.

In this paper we review the general theory for the movement of domain walls connecting two equivalent stable homogeneous solutions (labeled as phases) in two spatial dimensions and present in detail the perturbation theory originally developed in [14]. The paper is organized as follows: In section 2 we describe the type of systems to which our theory applies. In section 3 we derive a first order eikonal equation for the velocity of gently curved fronts and establish a criterion for the modulation instability of flat fronts. Then, in section 4 we extend the analysis close to the bifurcation point where the velocity vanishes to include nonlinear terms, and derive an amplitude equation for circular domain walls close to this point. In section 5 we summarize and discuss the different growth laws that can be observed in this systems. Finally, in section 6 we give some concluding remarks.

2 System description

We consider any system described by real N components vector field $\boldsymbol{\Psi}(\boldsymbol{x})$ whose dynamical evolution in two spatial dimensions can be written as

$$\partial_t \boldsymbol{\Psi} = D\nabla^2 \boldsymbol{\Psi} + \boldsymbol{W}(\boldsymbol{\Psi}, p)\,, \tag{1}$$

where the matrix D describes the spatial coupling, $\boldsymbol{W}$ is a local nonlinear function of the fields and p a control parameter. Equation (1) is invariant under translations and under the change $\mathcal{P} : \boldsymbol{x} \to -\boldsymbol{x}$ (parity). We also assume that it has a discrete symmetry $\mathcal{Z}$ that allows for the existence of two, and only two, equivalent stable homogeneous solutions, and that, in a 1d system, they are connected by stable Ising fronts $\boldsymbol{\Psi}_0(x, p)$. An Ising front is invariant with respect to $\mathcal{S} = \mathcal{Z}\mathcal{P}_0$, where the subscript $_0$ means that the reference frame for the spatial inversion is chosen at the center of the wall x_0 [20]. Thus, the 1d front (and equivalently a flat front in 2d) is stationary, $D\nabla^2 \boldsymbol{\Psi}_0 + \boldsymbol{W}(\boldsymbol{\Psi}_0, p) = 0$.

For the sake of clarity we will illustrate our general results throughout the paper on a prototypical model: the Parametrically driven Complex Ginzburg–Landau Equation (PCGLE). The PCGLE [21,22] is the generic amplitude equation for an oscillatory system parametrically forced at twice its natural frequency [15]:

$$\partial_t A = (1 + i\alpha)\nabla^2 A + (\mu + i\nu)A - (1 + i\beta)|A|^2 A + pA^*, \tag{2}$$

where μ measures the distance from the oscillatory instability threshold, ν is the detuning and $p > 0$ is the forcing amplitude. This model has been used to describe a light sensitive form of the Belousov–Zhabotinsky reaction [15,16].

The PCGLE is an example fulfilling the hypothesis required above. For $p \sim \nu \sim \alpha$ large compared to other parameters a pattern forming instability takes place for $p < p_h$, while for $p > p_h$ there are two equivalent stable homogeneous solutions (frequency locked solutions) (figure 1). In the PCGLE both Ising and Bloch walls can be observed. We restrict ourselves to parameter regions where the fronts connecting the two homogeneous solutions are of Ising type.

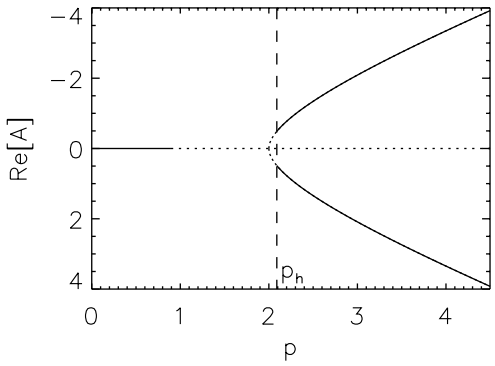

Fig. 1. Bifurcation diagram of the homogeneous solutions of the PCGLE for $\alpha = 2$, $\beta = 0$, $\nu = 2$ and $\mu = 0$. Solid lines indicate linearly stable solutions while dotted lines indicate solutions that are unstable under finite wavelength perturbations. For the parameter values considered, $p_h = 2.09$ (dashed line).

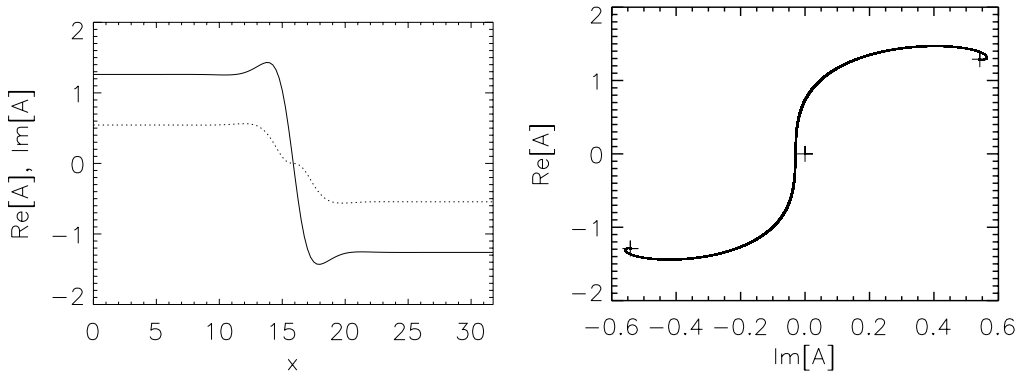

Fig. 2. A heteroclinic solution consisting of a Ising wall for $p = 2.75$. Other parameters as in figure 1. Left: Real part (solid line) and imaginary part (dotted line) of the complex field A as a function of x in the PCGLE. The center of the wall $x_0 = 16$ is the point where the two lines cross each other, which in this case corresponds to point where the field vanishes. Note the invariance with respect to $\mathcal{S} = \mathcal{Z}\mathcal{P}_0$. Right: The domain wall plotted in the A-complex plane. The crosses indicate the two equivalent homogeneous stable solutions and the zero unstable solution.

The real vector field describing the state of the system is $\mathbf{\Psi}(\boldsymbol{x}) = (\mathrm{Re}[A(\boldsymbol{x})], \mathrm{Im}[A(\boldsymbol{x})])$, the spatial coupling is described by the matrix $D = ((1,\alpha)^T, (-\alpha, 1)^T))$, $\mathcal{Z} = -I$ and $\mathbf{\Psi}_0(x)$ describes a Ising front connecting the two homogeneous solutions (we consider $p > p_h$). The front profile presents oscillatory tails as shown in figure 2. The 1d front profile $\mathbf{\Psi}_0$ is obtained by solving the 1d stationary equation of (2), namely

$$(1 + i\alpha)\frac{\mathrm{d}^2 A}{\mathrm{d}x^2} + (\mu + i\nu)A - (1 + i\beta)|A|^2 A + pA^* = 0\,, \tag{3}$$

where we impose first derivative equal to zero at each boundary. We then discretize the space and solve the set of coupled ordinary differential equations using a Newton method in which the transverse derivatives are computed in Fourier space [23–25].

3 Eikonal equation

In the reference frame moving with a front equation (1) becomes [26]:

$$D\partial_u^2 \mathbf{\Psi} + \left(v_n I + \frac{\kappa}{1+u\kappa} D\right)\partial_u \mathbf{\Psi} + \frac{u\kappa^2 \partial_\theta \kappa}{(1+u\kappa)^3} D\partial_\theta \mathbf{\Psi} + \frac{\kappa^2}{(1+u\kappa)^2} D\partial_\theta^2 \mathbf{\Psi} + \boldsymbol{W}(\mathbf{\Psi}, p) = \partial_t \mathbf{\Psi}, \tag{4}$$

where u is the coordinate normal to the front, s is the arclength of the line front, v_n is the normal front velocity, κ is the local curvature of the front line, $\theta = \kappa s$ is the azimuthal angle and I the identity matrix. We analyze the dynamics of slightly curved fronts $\boldsymbol{\Psi}(u,s,t)$ as a perturbation of the flat front $\boldsymbol{\Psi}_0(u)$

$$\boldsymbol{\Psi}(u,s,t) = \boldsymbol{\Psi}_0(u) + \boldsymbol{\Psi}_1(u,s,t). \tag{5}$$

We assume that (i) $\kappa w \ll 1$, with w the front width, (ii) in the moving frame the front profile depends at most weakly on t ($|\partial_t \boldsymbol{\Psi}| \ll |\kappa D \partial_u \boldsymbol{\Psi}|$) and (iii) κ is a function which depends at most weakly on s, thus $|\kappa \partial_\theta^2 \boldsymbol{\Psi}| \sim |\kappa \partial_\theta \boldsymbol{\Psi}| \ll |\partial_u \boldsymbol{\Psi}|$. Linearizing equation (4) around $\boldsymbol{\Psi}_0$ keeping only first order terms in κ and $\boldsymbol{\Psi}_1$ we have

$$M\boldsymbol{\Psi}_1 = -(v_n I + \kappa D)\partial_u \boldsymbol{\Psi}_0\,, \tag{6}$$

where $M^i_j = D^i_j \partial_u^2 + \delta_{\Psi^j} W^i|_{\boldsymbol{\Psi}_0,p}$. The last term is the functional derivative of the ith component of the nonlinear vector function $\boldsymbol{W}(\boldsymbol{\Psi},p)$ with respect to the jth component of the real vector field $\boldsymbol{\Psi}$. Due to the translational invariance of (1), which is broken by the presence of the domain wall, fronts have a neutrally stable Goldstone mode $\boldsymbol{e}_0$ ($M\boldsymbol{e}_0 = 0$), whose spatial profile is given by the gradient of the front $\boldsymbol{e}_0 \equiv \partial_u \boldsymbol{\Psi}_0$. Since the front is symmetric with respect to $\mathcal{S}$, its gradient $\boldsymbol{e}_0$ is antisymmetric. Due to the existence of the neutrally stable mode, M is singular and there exist a condition for equation (6) to have a solution, the so called solvability condition (see Appendix A in [27]). The condition is obtained multiplying on the left both sides of (6) by the null vector of $M^\dagger$, $\boldsymbol{a}_0$:

$$\int_{-\infty}^{\infty} \boldsymbol{a}_0 \cdot (v_n I + \kappa D)\boldsymbol{e}_0 \,\mathrm{d}u = 0. \tag{7}$$

Equation (7) leads to the eikonal equation

$$v_n = -\gamma(p)\kappa, \tag{8}$$

where

$$\gamma(p) \equiv \frac{1}{\Gamma}\int_{-\infty}^{\infty} \boldsymbol{a}_0 \cdot D\boldsymbol{e}_0 \,\mathrm{d}u\,, \tag{9}$$

and $\Gamma \equiv \int_{-\infty}^{\infty} \boldsymbol{a}_0 \cdot \boldsymbol{e}_0 \,\mathrm{d}u$. Γ vanishes at a Ising–Bloch transition [20]. Here we only consider parameter regions far away from any Ising–Bloch transition for which Γ is never zero. For a circular domain $\kappa = 1/R$ and

$$v_n = \dot{R} = -\gamma(p)/R\,. \tag{10}$$

From equation (6) one obtains that the front perturbation $\boldsymbol{\Psi}_1(u,t) = \kappa(t)\boldsymbol{\varphi}_1(u)$ is independent of s while the dependence on t comes only through κ. $\boldsymbol{\varphi}_1$ satisfies

$$M\boldsymbol{\varphi}_1 = -(-\gamma I + D)\boldsymbol{e}_0. \tag{11}$$

For systems such that the diffusion matrix is proportional to the identity, $D = dI$,

$$\gamma = \frac{d}{\Gamma}\int_{-\infty}^{\infty} \boldsymbol{a}_0 \cdot I\boldsymbol{e}_0 \,\mathrm{d}u = \frac{d}{\Gamma}\Gamma = d. \tag{12}$$

Thus, γ takes the constant value d independently of the profile of the front and any system parameter. In this case, the rhs of (11) vanishes and $\boldsymbol{\varphi}_1$ must be either zero or proportional to the Goldstone mode $\boldsymbol{e}_0$. Physically this means that the fronts translate without changing their radial profile. The front velocity is proportional to the curvature with opposite sign $v_n = -d\kappa$, which is the well known Allen–Cahn law [3,5]. This law implies a coarsening regime with a $t^{1/2}$ growth law and shrinking of circular domains following $R(t) = \sqrt{R(0)^2 - \gamma t}$, as obtained from (10) (figure 4).

In general, $D = dI + C$ with a non zero matrix C, so that

$$\gamma = d + \frac{1}{\Gamma}\int_{-\infty}^{\infty} \boldsymbol{a}_0 \cdot C\boldsymbol{e}_0 \,\mathrm{d}u. \tag{13}$$

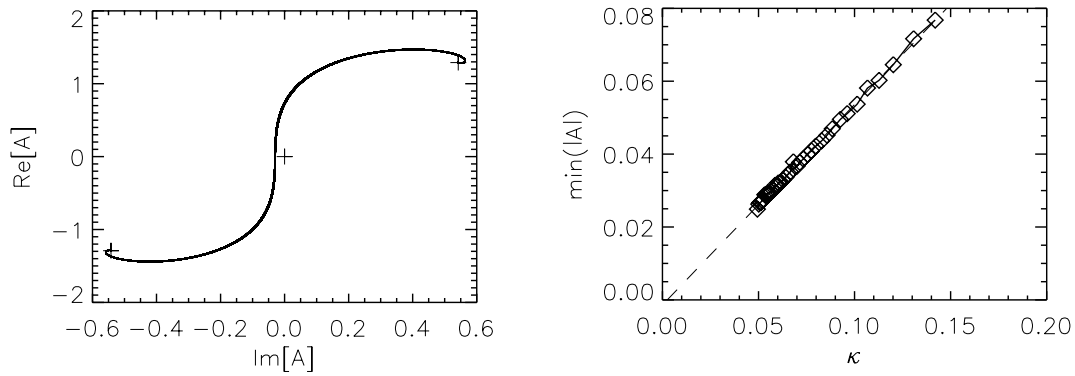

Fig. 3. Left: wall profile of a gently curved front in 2D plotted in the A-complex plane. The symbols correspond to the zero solution and the two non-trivial homogeneous equivalent solution. The difference between the curved front and the flat wall (figure 2) is the effect of the deformation due to the first order correction $\mathbf{\Psi}_1$. The distance of the center of walls from the zero solution, given by $\min|A|$, is a measure of the deformation and is plotted in the right panel as a function of the curvature for a shrinking circular domain. The linear dependence predicted theoretically is clear. The dashed line is a linear fitting of the data from the simulations.

C leads to a contribution to γ that depends on the profile of the front $\mathbf{\Psi}_0$ and therefore, on the system parameters. From equation (11) we have that $\boldsymbol{\varphi}_1$ is no longer proportional to the Goldstone mode. This means that the transverse profile of the front is now deformed by the curvature. Since $\mathbf{\Psi}_1(u,t) = \kappa(t)\boldsymbol{\varphi}_1(u)$, the amount of deformation is proportional to the curvature. Due to the deformation, real and imaginary parts of the field does not vanish simultaneously at any point of the wall, so $|A|$ is always positive. In fact, the minimum of $|A|$, which takes place at the center of the wall, can be considered a good measure of the deformation. As shown in figure 3) the deformation grows linearly with the curvature as predicted. While deformation can be interpreted as the original flat Ising wall getting chirality, this deformed Ising front must no be confused with a Bloch wall resulting of a symmetry breaking bifurcation and which has chirality even in 1D. Thus, for example, in optical systems the experimental observation of fronts for which the intensity does not vanish at the center [28] does not necessarily imply that these are Bloch fronts if the fronts have local curvature.

The d contribution is generally positive and, for wide parameter regions, γ is also positive. Here flat walls are stable and the Allen-Cahn law still applies [10,24] (figure 4).[1] Circular domains shrink but in the parameter regions where the γ coefficient takes moderated values the 1d interaction due to presence of oscillatory tails in the front may prevent the droplet to disappear forming a localized structure (LS) (figure 5).

The crucial point is that for some parameter values the contribution to γ due to C may be negative and larger than d. γ changes sign and a bifurcation occurs. Figure 6 shows the value of γ versus p for the PCGLE.

The value of p for which $\gamma = 0$ identifies the bifurcation point p_c. This is particularly relevant in nonlinear optics where the spatial coupling is diffractive and therefore $d = 0$. For $\gamma < 0$ the velocity has the same sign of the curvature leading to the growth of any perturbation of the flat wall. The condition for vanishing γ, $\int_{-\infty}^{\infty} \boldsymbol{a}_0 \cdot D\boldsymbol{e}_0 \, \mathrm{d}u = 0$, is in fact the criterion for the modulational instability of a flat front. Modulational instabilities in fronts connecting two equivalent homogeneous states have been studied in [10,15,30] (figure 7). Starting from a

[1] Numerical simulations have been performed on a 256×256 square grid using a pseudospectral method as in R. Montagne et al., Phys. Rev. E **56**, 151 (1997). Linear terms are treated exactly in Fourier space while a second order in time approximation is used for nonlinear terms. This automatically implement periodic boundary conditions. The system size is taken large enough so that no finite size effects influence the calculation of the growth rate of circular domains. Throughout the paper $\Delta x = 0.25$ and $\Delta t = 0.1$.

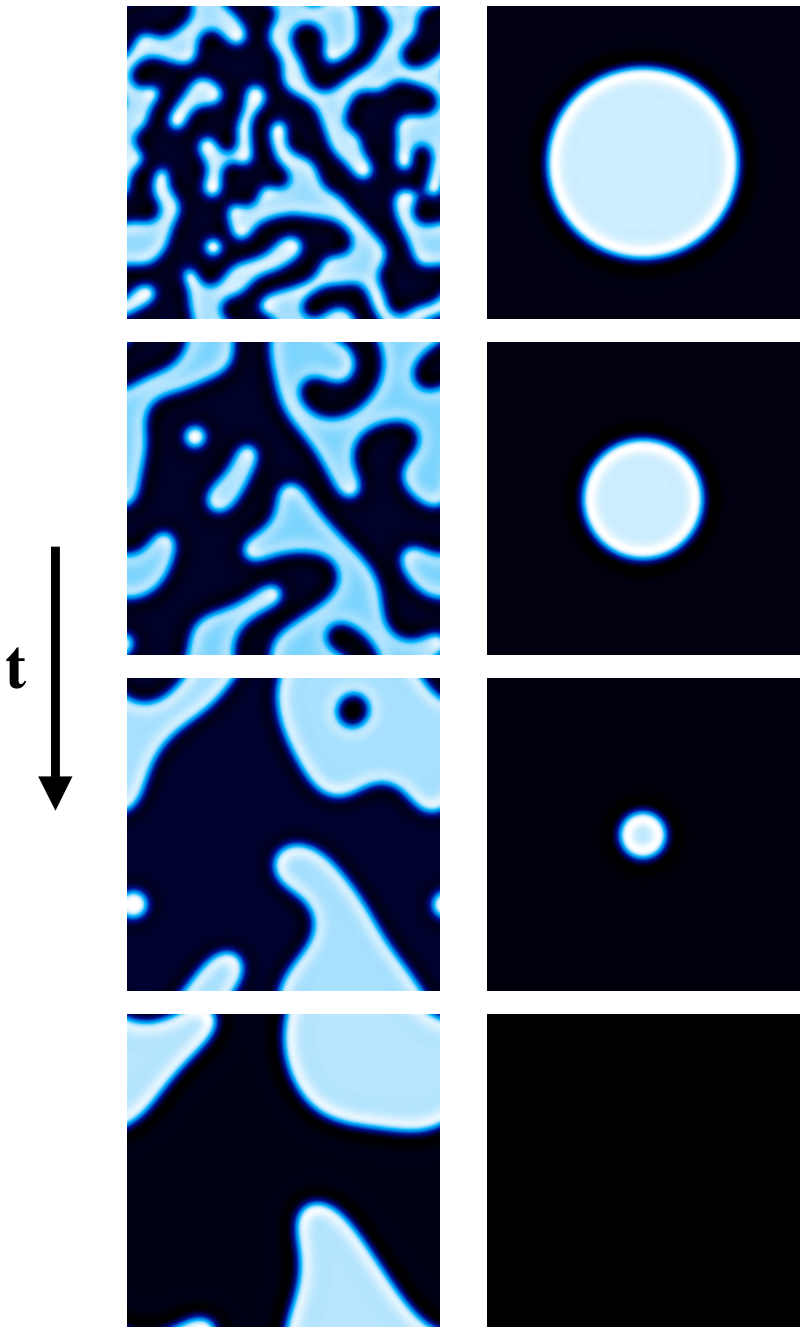

Fig. 4. Snapshots corresponding to the time evolution of the real part of the complex field A for the parametrically driven complex Ginzburg–Landau equation in the domain coarsening regime ($p = 2.9$ for which $\gamma > 0$). Left: evolution starting from random initial conditions. Right: evolution of a circular domain of the phase $A = (1.3455, -0.5382)$ in a background of phase $A = (-1.3455, 0.5382)$. The reverse case would let to exactly the same dynamics as the two solutions are equivalent. The total time of the sequence is 1000 time units.

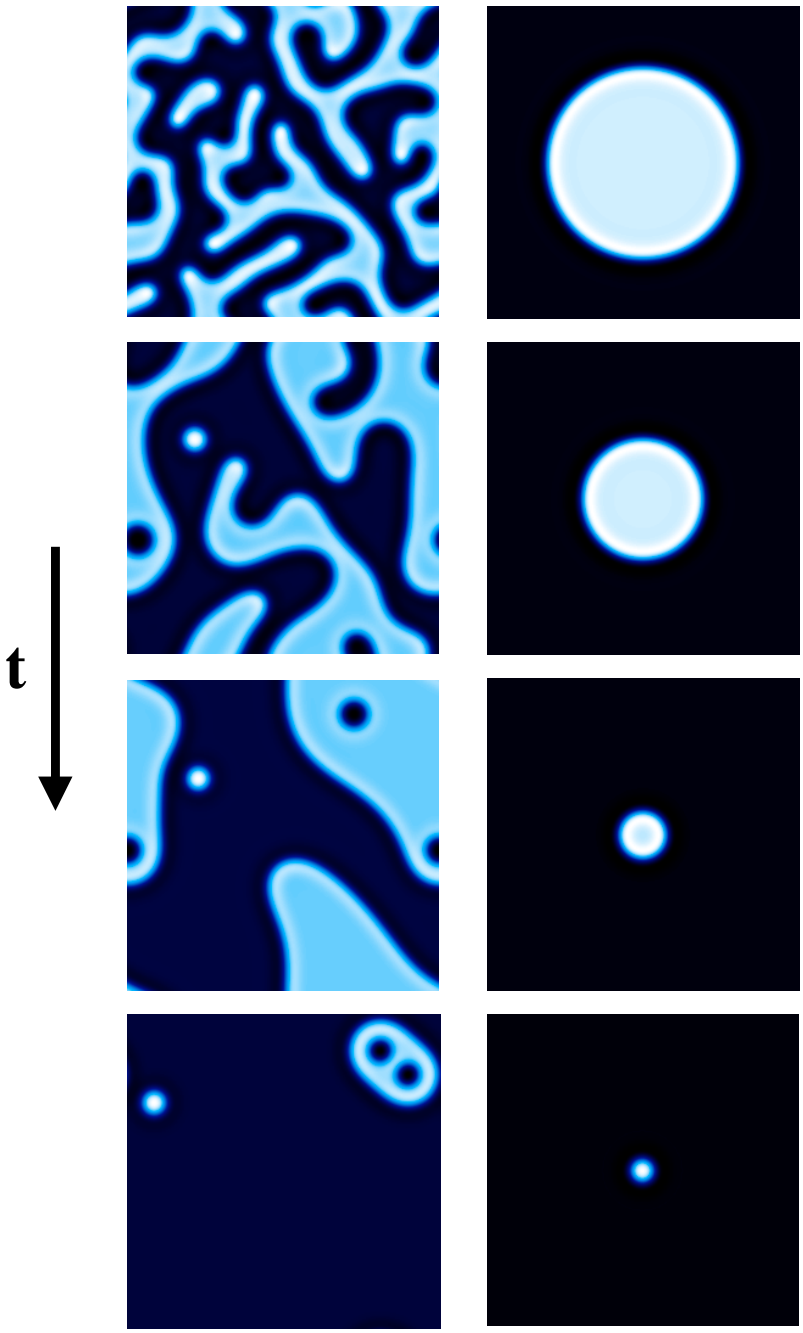

Fig. 5. The same as figure 4 in the regime of formation of LS ($p = 2.7$ for which $\gamma > 0$ but small enough to not overcome the oscillatory tails interaction). Here the total integration time is 2000 time units.

random initial condition, the system develops labyrinthine patterns [10,15,17]. Also, a circular domain grows like (10) until its boundary breaks up because of the modulational instability leading to the formation of a labyrinthine pattern (figure 8).

The values of γ shown in figure 6 have been calculated from its definition equation (9). From the discretized profile $\mathbf{\Psi}_0$ obtained from equation (3) we evaluate the operator M, which now takes the form of a $N \times N$ matrix with N the number of grid points. The null mode of $M^\dagger$ is easily obtained by finding the eigenmodes of the transposed of the matrix M. This process

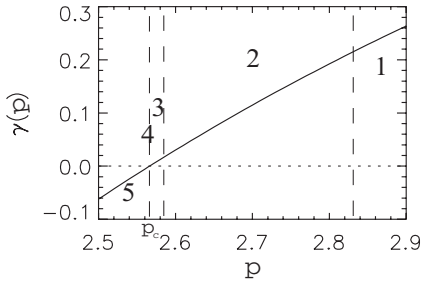

Fig. 6. γ as function of p calculated from equation (9) for the PCGLE. Parameters taken as in figure 1. γ becomes zero at $p_c = 2.56629$. The regions labeled with different numbers and separated by dashed vertical lines indicate the parameter values for which different asymptotic regimes are found: 1) coarsening, 2) formation of localized structures, 3) stable droplets, 4) $t^{1/4}$ growth law, and 5) labyrinthine patterns.

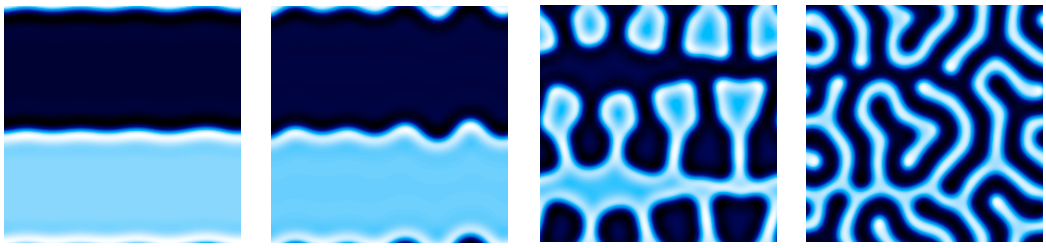

Fig. 7. Images showing the development of a modulational instability of a flat wall for the PCGLE. The time increases from left to right.

allows us to calculate γ with very high accuracy much faster than following the time evolution of a 2d circular droplet from a numerical integration of equation (2).

4 Amplitude equation for the curvature: Stable droplets

In the previous section we have developed a perturbation theory at first order in the curvature κ. However, for values of the control parameter p close to p_c, where the proportionality coefficient γ between the velocity and the curvature vanishes (modulational instability of a domain wall), higher order contributions in κ, that have been neglected in the previous sub-section, may become relevant. In order to study these nonlinear contributions we perform a multiple scale analysis in ϵ of equation (4). We start considering the case of a circular domain wall (for which $v_n = -\dot{\kappa}/\kappa^2$). Assuming the following scaling:

$$\begin{aligned} &p = p_c + \epsilon p_1, \qquad \boldsymbol{\Psi} = \boldsymbol{\Psi}_0 + \epsilon^{1/2}\boldsymbol{\Psi}_1 + \epsilon\boldsymbol{\Psi}_2 + \epsilon^{3/2}\boldsymbol{\Psi}_3, \\ &\kappa = \epsilon^{1/2}\kappa_1 \quad \text{and} \quad \partial_t = \epsilon^2\partial_T, \end{aligned} \tag{14}$$

at order $\epsilon^{1/2}$ we obtain

$$M\boldsymbol{\psi}_1 = -\kappa_1 D\boldsymbol{e}_0. \tag{15}$$

Now the solvability condition is $\int_{-\infty}^{\infty} \boldsymbol{a}_0 \cdot D\boldsymbol{e}_0 \, \mathrm{d}r = 0$, which is precisely the criterion for the modulational instability of a domain wall, and therefore is automatically satisfied at p_c. Then a solution of (15) can be found:

$$\boldsymbol{\Psi}_1 = \kappa_1 \boldsymbol{\varphi}_1 \tag{16}$$

with $M\boldsymbol{\varphi}_1 = -D\boldsymbol{e}_0$. At order ϵ we obtain

$$M^i_j \Psi^j_2 = -p_1 \partial_p W^i|_0 - \kappa_1^2 D^i_j(\partial_u \varphi^j_1 - u e^j_0) - \frac{\kappa_1^2}{2}\delta_{\Psi^j\Psi^k} W^i|_0 \varphi^j_1 \varphi^k_1 \tag{17}$$

where $|_0$ means evaluated at $\boldsymbol{\Psi}_0$ and p_c, and the solvability condition is

$$\int_{-\infty}^{\infty} a_{0i} \left[p_1 \partial_p W^i|_0 + \kappa_1^2 D^i_j(\partial_u \varphi^j_1 - u e^j_0) + \frac{\kappa_1^2}{2}\delta_{\Psi^j\Psi^k} W^i|_0 \varphi^j_1 \varphi^k_1 \right] = 0. \tag{18}$$

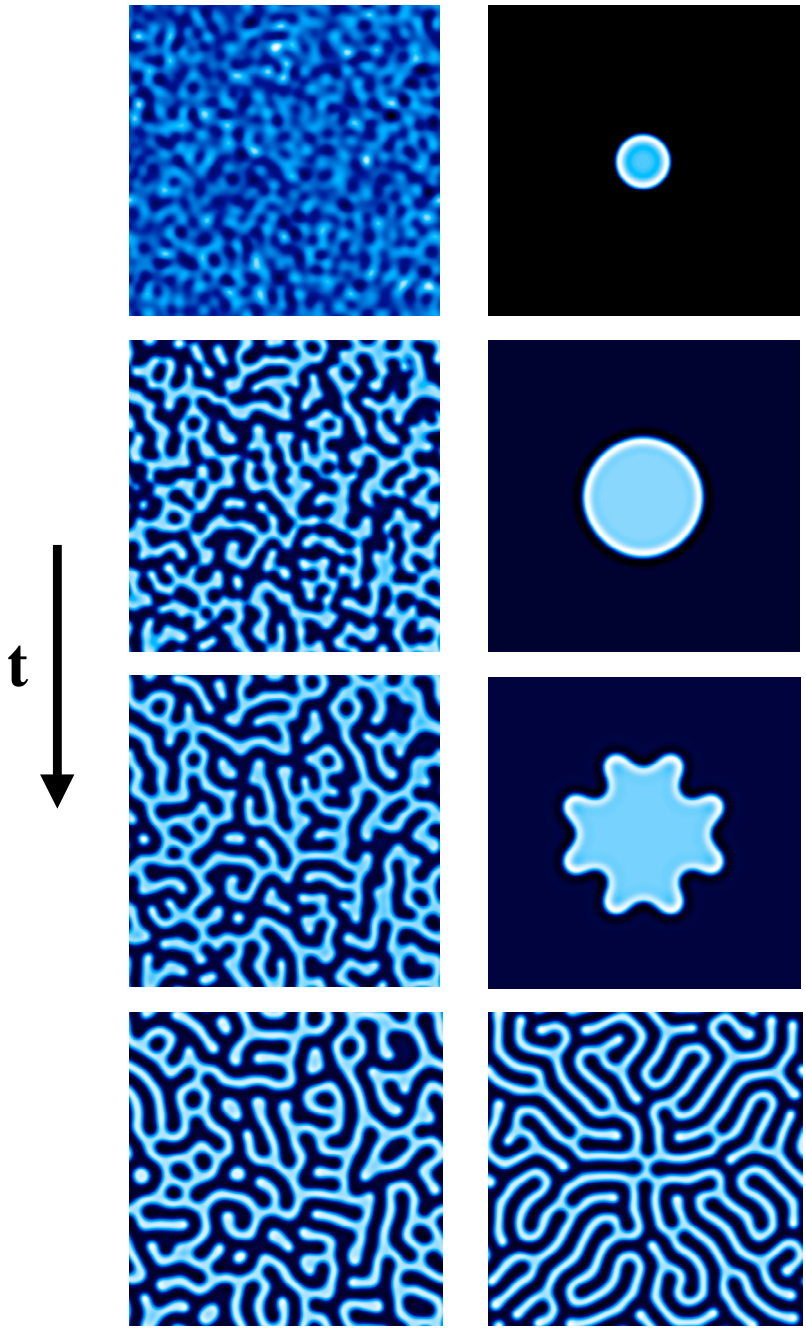

Fig. 8. The same as figure 4 in the regime of formation of labyrinthine structures (region 5 in figure 6, for which $\gamma < 0$).

$\boldsymbol{a}_0$ has the same symmetry with respect to $\mathcal{S}$ as the Goldstone mode $\boldsymbol{e}_0$, namely it is antisymmetric, while the expression in brackets is symmetric. Therefore the integral (18) vanishes, and the solvability condition at this order is always fulfilled. Then, a solution of the form

$$\boldsymbol{\Psi}_2 = p_1 \boldsymbol{\varphi}_2 + \kappa_1^2 \boldsymbol{\varphi}_3 \tag{19}$$

with $M\boldsymbol{\varphi}_2 = -\partial_p \boldsymbol{W}|_0$ and $M^i_j\varphi^j_3 = -D^i_j(\partial_r\varphi^j_1 - re^j_0) - \frac{1}{2}\delta^j_\Psi \Psi_k W^i|_0 {\varphi_1}^{j}{\varphi_1}^{k}$ can be found. To obtain an amplitude equation for the curvature κ_1 we have to go to order $\epsilon^{3/2}$. We have

$$M^i_j\Psi^j_3 = \frac{\partial_T\kappa_1}{\kappa_1^2}e^j_0 - p_1\kappa_1(D^i_j\partial_r\varphi^j_2 + \delta_{\Psi^j}\partial_p W^i|_0\varphi^j_1 + \delta_{\Psi^j\Psi^k}W^i|_0\varphi^j_1\varphi^k_2)$$
$$-\kappa_1^3[D^i_j(\partial_r\varphi^j_3 - r\partial_r\varphi^j_1 + r^2e^j_0) + \delta_{\Psi^j\Psi^k}W^i|_0\varphi^j_1\varphi^k_3 + \delta_{\Psi^j\Psi^k\Psi^l}W^i|_0\varphi^j_1\varphi^k_1\varphi^l_1/6]\,. \tag{20}$$

The solvability condition is:

$$\frac{\partial_T\kappa_1}{\kappa_1^2} = c_1p_1\kappa_1 + c_3\kappa_1^3 \tag{21}$$

with

$$c_1 = \frac{1}{\Gamma}\int_{-\infty}^{\infty} a_{0i}(D^i_j\partial_r\varphi^j_2 + \delta_{\Psi^j}\partial_p W^i|_0\varphi^j_1 + \delta_{\Psi^j\Psi^k}W^i|_0\varphi^j_1\varphi^k_2)\,\mathrm{d}r \tag{22}$$

$$c_3 = \frac{1}{\Gamma}\int_{-\infty}^{\infty} a_{0i}[D^i_j(\partial_r\varphi^j_3 - r\partial_r\varphi^j_1 + r^2e^j_0) + \delta_{\Psi^j\Psi^k}W^i|_0\varphi^j_1\varphi^k_3 + \delta_{\Psi^j\Psi^k\Psi^l}W^i|_0\varphi^j_1\varphi^k_1\varphi^l_1/6]\mathrm{d}r. \tag{23}$$

Equation (21) is written in the scaled curvature (14). Undoing the scaling we get

$$\frac{\partial_t\kappa}{\kappa^2} = c_1(p - p_c)\kappa + c_3\kappa^3. \tag{24}$$

For the radius of a circular domain ($R = 1/\kappa$) equation (24) becomes

$$\partial_t R = -c_1(p - p_c)/R - c_3/R^3. \tag{25}$$

$c_1 > 0$ since $\gamma = c_1(p - p_c)$, and we are considering $\gamma > 0$ for $p > p_c$. If c_3 is negative (supercritical bifurcation) our analysis predicts just above p_c the existence of stable stationary circular domains (SD) with a very large radius R_0:

$$R_0 = \frac{1}{\sqrt{p - p_c}}\sqrt{\frac{-c_3}{c_1}}. \tag{26}$$

In figure 9 we show the form of the SD for the PCGLE. At the SD center the field closely approaches the value of one of the homogeneous solutions so the wall of this structure is very close to a heteroclinic orbit between the two homogeneous states (figure 9 (right)). The radius of the SD diverges to infinity at p_c. Figure 10 displays the radius of the SD and that of the LS calculated by solving numerically

$$(1 + i\alpha)\left(\partial_r^2 + \frac{1}{r}\partial_r\right)A + (\mu + i\nu)A - (1 + i\beta)|A|^2A + pA^* = 0$$

as done for equation (3).

Figure 10 (right) shows the linear dependence of $1/R_0^2$ with p as predicted by (26). In spite of the fact that there is a smooth transition from LS to SD (figure 10 (left)), these two localized states are intrinsically different. As the radius of the stable droplets is so large, the oscillatory tails interaction, responsible for the existence of LS (figure 11), does not play any role in the SD. The stabilization mechanism comes from the counterbalance between the R^{-3} contribution to the front velocity and the shrinking due to the R^{-1} contribution.[2] If $c_3 > 0$ (subcritical bifurcation) there would exist an unstable circular domains with radius R_0 just below p_c. However, we have never encountered this situation.

[2] Crossover between different growth laws has been found in systems with conserved order parameter [31]. In that case, however, the coefficients have the same sign and there is no stationary radius for the domains.

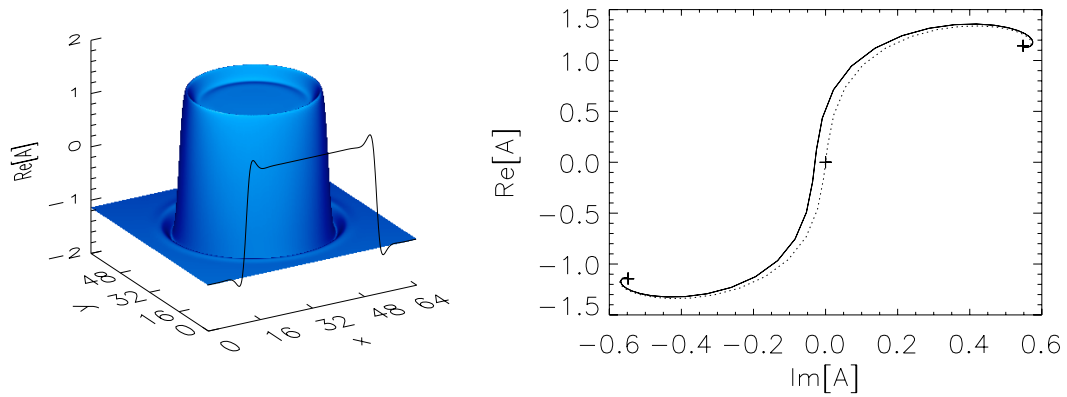

Fig. 9. Left: spatial dependence and transverse section of a stable droplet. Right: the wall of the structure plotted in the A-complex plane (solid line). The 1d wall (dotted line) is also plotted for comparison with the wall of the stable droplet. The crosses indicate the two equivalent homogeneous solutions and the zero solution. Note that the profile of the wall of the stable droplet is slightly deformed with respect to the 1d wall due to the first order correction $\mathbf{\Psi}_1$.

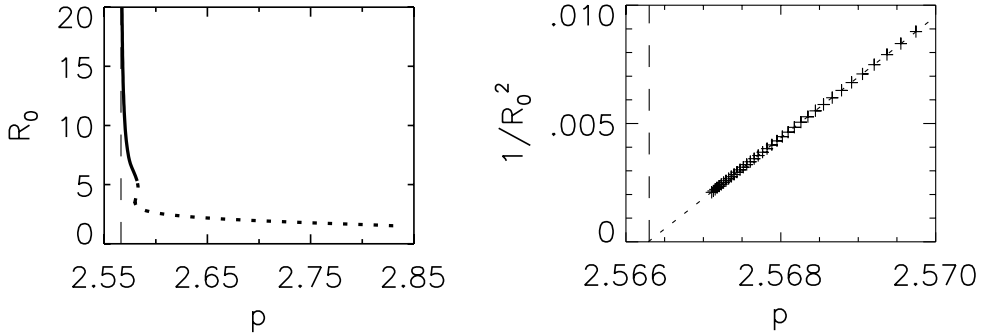

Fig. 10. Left: radius of SD (solid line) and LS (dotted line) as a function of the forcing p. Right: linear dependence of $1/R_0^2$ with p close to the bifurcation point p_c (dashed line) as predicted by (26).

Another interesting feature of the nonlinear contributions of the curvature to the front velocity is the growth law of the circular domains at p_c. At p_c, equation (25) becomes

$$\partial_t R = -c_3/R^3, \tag{27}$$

and any circular domain of one solution embedded in the other grows as

$$R(t) = (R^4(0) - 4c_3 t)^{1/4}, \tag{28}$$

and, asymptotically, the radius follows the power law $R(t) \sim t^{1/4}$. In figure 12 we show the time evolution of the radius of a circular domain at p_c for the PCGLE. The numerical integration of equation (2) (circles) fits nicely the theoretical dependence predicted by equation (28) (solid line). Note that, since we calculate the value of c_3 from the solvability condition, we are able to predict not only the asymptotic power law but also the growth at earlier stages.

Close to p_c, in the regime of existence of the SD, there is no asymptotic power law of domain growth since at very long times the SD is formed stopping the growth process. During the transient, an initially small (very large) circular domain will grow (shrink) following (25) (figure 13).

So far we have considered the dynamics of domains with radial symmetry. When the system evolves from random initial conditions other dynamical mechanisms come into play. The main non-radially symmetric contribution to the velocity comes from the variation of the curvature

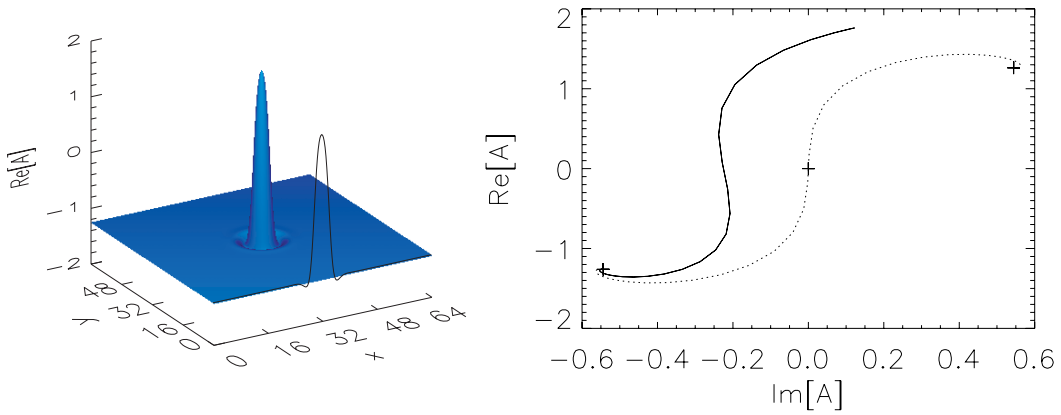

Fig. 11. Left: spatial dependence and transverse section of a LS. Right: a cross-section of the LS plotted in the A-complex plane (solid line). The 1d wall (dotted line) is also plotted for comparison with the wall of the LS. The crosses indicate the two equivalent homogeneous solutions and the zero solution. Note that a LS can not be considered as a heteroclinic connection between the two homogeneous solutions.

along the front. Taking this effect into account, we can derive an amplitude equation for the normal velocity v_n. Using the fact that for circular domains $v_n = \partial_t \kappa/\kappa^2$, which is of order $\epsilon^{1/2}$, we now assume the scaling $v_n = \epsilon^{1/2} v_{n1}$. We obtain at order $\epsilon^{3/2}$ an additional term for the solvability condition with respect to the radially symmetric case given by (21):

$$c_2 \kappa_1^2 \partial_\theta^2 \kappa_1, \tag{29}$$

where $c_2 = \frac{1}{\Gamma} \int_{-\infty}^{\infty} \boldsymbol{a_0} \cdot D\boldsymbol{\varphi}_1 \mathrm{d}r$. Thus,

$$v_{n1} = c_1 p_1 \kappa_1 + c_2 \kappa_1^2 \partial_\theta^2 \kappa_1 + c_3 \kappa_1^3. \tag{30}$$

Undoing the scaling, the front velocity becomes

$$v_n = -c_1 (p - p_c)\kappa - c_2 \kappa^2 \partial_\theta^2 \kappa - c_3 \kappa^3. \tag{31}$$

Consistently with our approximations, $\partial_\theta^2 \kappa$ will change at most at order κ^0, so the non-radial contribution is at least of order κ^2. For p/nep_c the first term on the right hand side of equation (31) dominates the dynamics and the system exhibits a $t^{1/2}$ growth law. At p_c, $c_1(p - p_c)\kappa$ vanishes, and the term given by $-c_2 \kappa^2 \partial_\theta^2 \kappa$ may be dominant compared with $c_3 \kappa^3$. The front velocity is then proportional to κ^2. However, for any closed boundary

$$\int_0^{2\pi} \partial_\theta^2 \kappa = \partial_\theta \kappa|_0^{2\pi} = 0, \tag{32}$$

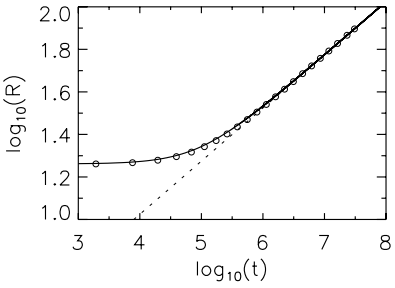

Fig. 12. Growth of a circular domain as function of the time at $p = p_c$. Symbols correspond to the numerical integration of equation (2), while the solid line is the theoretical prediction (28) with $c_3 = 0.3129$ calculated from (23). The dotted line has a slope 1/4 showing the asymptotic behavior.

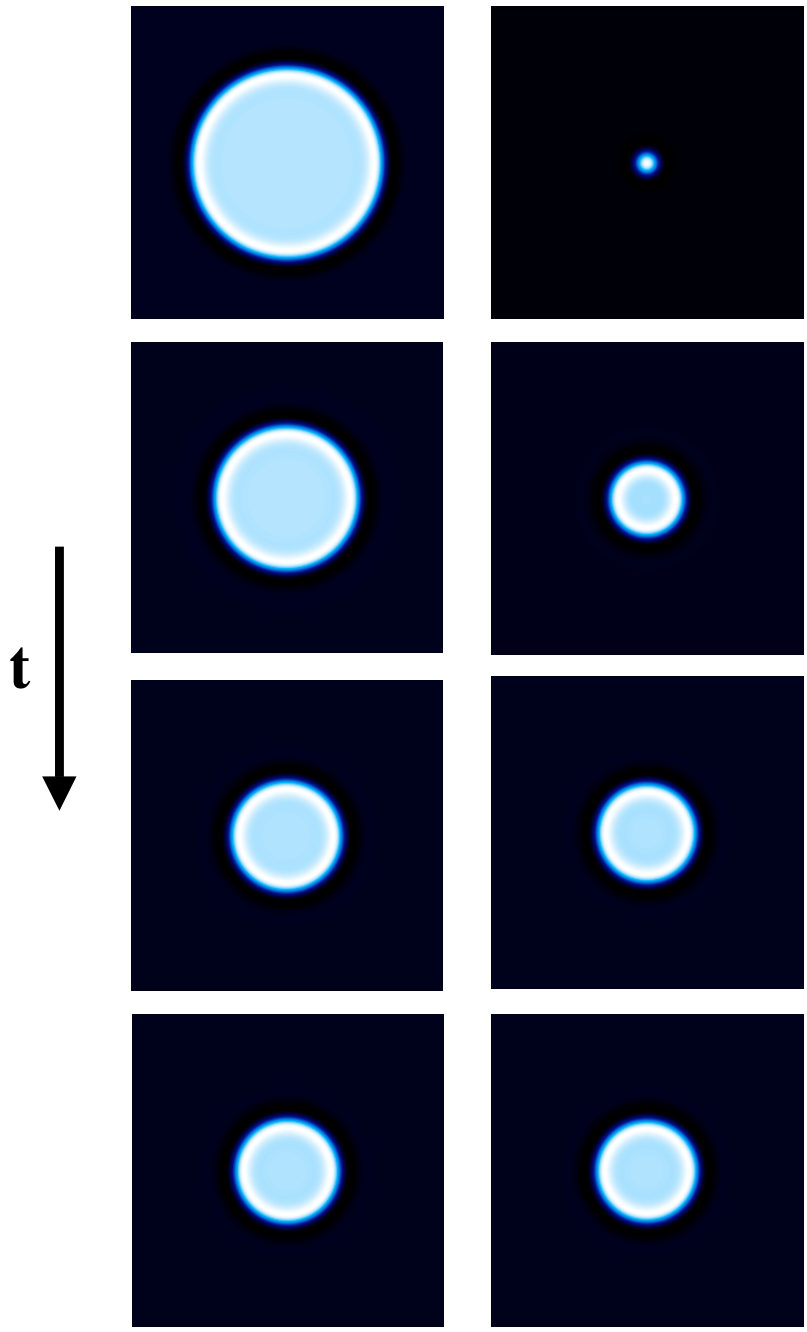

Fig. 13. Snapshots corresponding to the time evolution of a very large and a small circular domains for the parametrically driven complex Ginzburg–Landau equation in the regime of existence of stable droplets.

so $\partial_\theta^2 \kappa$ has to be positive in some parts of the wall and negative in others, therefore, this term does not lead to an asymptotic growth law. If $c_2 < 0$, which is the case for the PCGLE, this term tends to reduce the curvature differences, so at p_c an arbitrarily shaped domain first becomes circular until the contribution of $\partial_\theta^2 \kappa$ vanishes and then the circular domain grows as $R(t) \sim t^{1/4}$ due to the c_3 term. Figure 14 shows the time evolution of an arbitrarily shaped domain at $p = p_c$ for the PCGLE.

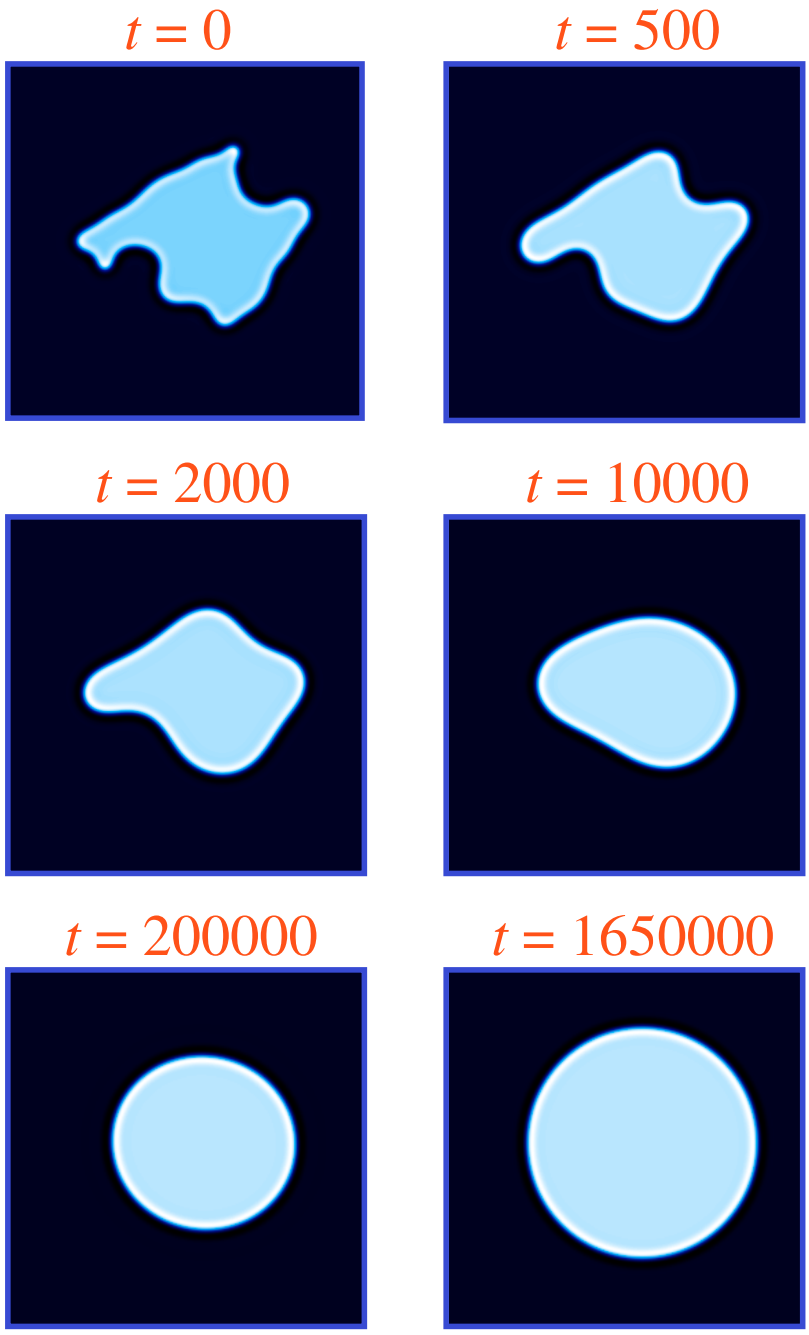

Fig. 14. Evolution of an arbitrarily shaped domain at $p = p_c$.

At early stages we can observe the reduction of curvature differences along the front due to the nonradially symmetric contribution, until the domain become circular. Then, the contribution from the $\partial_\theta^2 \kappa$ term vanishes and the cubic radial symmetric term makes the circular domain to grow with a $t^{1/4}$ power law (a much slower time scale).

5 Scaling laws

The determination of growth laws allows to establish from both theoretical and experimental data the mechanism that governs the dynamics of interfaces. In the previous sections we have

explained different growth processes in a framework which allow to include many non-potential systems, for which interface dynamics is, in general, quite poorly understood. In the generic situation of domain wall motion driven by curvature in which the proportionality coefficient γ between wall velocity and curvature changes sign at a bifurcation point, we have identified five different dynamical regimes with different growth laws (see figure 6). For γ positive and large (region 1) there is a coarsening regime where the growth of domains is given by the Allen–Cahn $t^{1/2}$ power law. For γ positive but small (region 2), localized structures can be formed as a consequence of the interactions of the tails of the fronts. The formation of these localized structures halt the self-similar evolution and, strictly speaking, there is no power law in this regime. The Allen–Cahn $t^{1/2}$ law can still be observed, however, in transient regimes. Just above the bifurcation point p_c (region 3), the amplitude equation for the curvature predicts the existence of stable nonlinear solutions, the stable droplets. Nonlinear dynamics of the curvature leads to growth laws different from the Allen–Cahn $t^{1/2}$ power law. The existence of a large characteristic length given by the radius of the stable droplet destroys the possibility of self-similar evolution in this regime. Exactly at the bifurcation point (point 5), however, the radius of the stable droplets become infinite and there is not a characteristic length in the system. A $t^{1/4}$ growth law is then obtained. Finally, for $\gamma < 0$ (region 5), circular domain walls growth with a $t^{1/2}$ power law, however domain walls are modulationally unstable leading to the formation of labyrinthine patterns. No self-similar evolution is then observed.

Our results are not based only on numerical simulation but come from a rigorous analysis which allow us to show what growth law can be found in each region of the parameter space and in which regions the growth rate of a domain does not follow a power law. Growth laws of the form $t^{1/3}$ do not appear in these systems. This result was obtained numerically [12,13], probably because the measurement was done in transient regimes where the asymptotic growth rate was not yet reached. The $t^{1/2}$ power law have been recently experimentally observed in two non-variational systems: a chemical reaction [16], described by the PCGLE, and a nonlinear optical system [32].

6 Concluding remarks

Our results are universal in that any 2d system with a modulational instability of a flat front connecting two equivalent homogeneous states displays similar droplets and dynamics independently of the nature of the coexisting phases. Such systems can be found in fields asb diverse as hydrodynamics, chemical reactions, material science and nonlinear optics. Transitions from coarsening to labyrinthine regimes has been observed experimentally in reaction diffusion [15,16] and optical [17,32] systems. The theory we presented in detail here predicts a novel kind of localized structures, the stable droplets, which owe their stability to the interplay between curvature and nonlinear effects, and therefore do not exist in 1d systems. Evidence of the existence of this objects is also present in [16]. Particularly relevant is the field of nonlinear optics, where the criterion for the modulational instability of a domain wall can be easily reached due to the diffractive coupling between real and imaginary parts of the complex field amplitude. We have applied our results to a model for a self-defocusing vectorial Kerr cavity with linearly polarized input field and to a model for a optical parametric oscillator. We have shown that in both cases there exist stable circular domains [33]. For the vectorial Kerr resonator these domains are in fact polarization domains, cavity polarization solitons, while for the optical parametric oscillator they are domains of opposite phase. This offers two different possibilities for addressing and manipulating cavity solitons. We have also shown that stable droplets nucleate out of dark ring cavity solitons but can coexist with dark ring cavity solitons in the parameter space. This fact may be exploited in increasing the information capacity of these devices by using the stable droplets and dark ring cavity solitons to encode separate information.

In real systems the perfect symmetry that makes the two homogeneous solutions equivalent is typically broken. For small asymmetries, however, the general theory can be generalized to include this effect changing slightly the scenario presented here [34].

We acknowledge financial support from MEC(Spain) through project CONOCE2 (FIS2004-00953).

References

1. P.D. Woods, A.R. Champneys, Physica D **129**, 147 (1999)
2. P. Coullet, C. Riera, C. Tresser, Phys. Rev. Lett. **84**, 3069 (2000)
3. J.D. Gunton, M.S. Miguel, P. Sahni, *Phase Transitions and Critical Phenomena*, edited by C. Domb, J. Lebowitz (Academic Press, New York, 1983), Vol. 8, p. 269
4. A. Bray, Adv. Phys. **43**, 357 (1994)
5. S.M. Allen, J.W. Cahn, Acta Metall. **27**, 1085 (1979)
6. E. Meron, Phys. Rep. **218**, 1 (1992)
7. M.C. Cross, D.I. Meiron, Phys. Rev. Lett. **75**, 2152 (1995)
8. C. Josserand, S. Rica, Phys. Rev. Lett. **69**, 1215 (1997)
9. R. Gallego, M.S. Miguel, R. Toral, Phys. Rev. E **58**, 3125 (1998)
10. R. Gallego, M.S. Miguel, R. Toral, Phys. Rev. E **61**, 2241 (2000)
11. G.-L. Oppo, A.J. Scroggie, W. Firth, J. Opt. B **1**, 133 (1999)
12. M. Tlidi, P. Mandel, R. Lefever, Phys. Rev. Lett. **81**, 979 (1998); M. Tlidi, P. Mandel, M. Le Berre, E. Ressayre, A. Tallet, L. Di Menza, Opt. Lett. **25**, 487 (2000); M. Tlidi, P. Mandel, Europhys. Lett. **44**, 449 (1998)
13. M. Le Berre, E. Ressayre, A. Tallet, J. Opt. B **2**, 347 (2000)
14. D. Gomila, P. Colet, M.S. Miguel, G.-L. Oppo, Phys. Rev. Lett. **87**, 194101 (2001)
15. V. Petrov, Q. Ouyang, H.L. Swinney, Nature **388**, 655 (1997)
16. B. Marts, K. Martinez, A. Lin, Phys. Rev. E **70**, 056223 (2004)
17. V.B. Taranenko, K. Staliunas, C.O. Weiss, Phys. Rev. Lett. **81**, 2236 (1998)
18. K. Ouchi, H. Fujisaka, Phys. Rev. E **54**, 3895 (1996)
19. K. Staliunas V.J. Sánchez-Morcillo, Phys. Lett. A **241**, 28 (1998); V.J. Sánchez-Morcillo, K. Staliunas Phys. Rev. E **60**, 6153 (1999)
20. D. Michaelis, U. Peschel, F. Lederer, D.V. Skryabin, W.J. Firth, Phys. Rev. E **63**, 066602 (2001)
21. P. Coullet, J. Lega, B. Houchmanzadeh, J. Lajzerowicz, Phys. Rev. Lett. **65**, 1352 (1990)
22. P. Coullet K. Emilsson, Physica D **61**, 119 (1992)
23. W.J. Firth, G.K. Harkness, Asian J. Phys. **7**, 665 (1998)
24. G.-L. Oppo, A.J. Scroggie, W. Firth, Phys. Rev. E **63**, 066209 (2001)
25. J.M. McSloy, W.J. Firth, G.K. Harkness, G.-L. Oppo, Phys. Rev. E **66**, 046606 (2002)
26. H. Tutu, Phys. Rev. E **56** 5036 (1997)
27. M.C. Cross, P.C. Hohenberg, Rev. Mod. Phys. **65**, 851 (1993)
28. Ye. Larionova, U. Peschel, A. Esteban-Martin, J. G. Monreal, C.O. Weiss, Phys. Rev. E **69**, 033803 (2004)
29. U. Peschel, D. Michaelis, C. Etrich, F. Lederer, Phys. Rev. E **58**, R2745 (1998)
30. A. Hagberg, A. Yochelis, H. Yizhaq, C. Elphick, L. Pismen, E. Meron, Physica D **217**, 186 (2006)
31. A.M. Lacasta, A. Hernández-Machado, J.M. Sancho, R. Toral, Phys. Rev. B **45**, 5276 (1992)
32. M. Pesch, T. Ackemann, D. Gomila, G.-L. Oppo, W.J. Firth, W. Lange (2007) (preprint)
33. D. Gomila, P. Colet, M. S. Miguel, A.J. Scroggie, G.-L. Oppo, J. Quant Electron. **39**, 238 (2003)
34. D. Gomila, P. Colet, M. S. Miguel, G.-L. Oppo, J. Opt. B **6**, S265 (2004)